Modeling Of Dust-Particle Dynamics, Transport, And Impact On Tokamak Plasma Performance

S. I. Krasheninnikov 1), R. D. Smirnov 1), D. J. Benson 1), A. Yu. Pigarov 1), T. K. Soboleva 2), T. D. Rognlien 3), M. Rosenberg 1), V. I. Shevchenko 1), P. K. Shukla 4), and D. A. Mendis 1)

1) University Of California At San Diego, La Jolla, California, USA
2) ICN, Universidad Nacional Autónoma De México, México D. F., México
3) Lawrence Livermore National Laboratory, Livermore, California, USA
4) Ruhr–Universität Bochum, Bochum, Germany

e-mail contact of main author: skrash@mae.ucsd.edu

Abstract. Recent theoretical developments on kinetics of volumetric growth and evaporation of dust particles due to dust-plasma interactions, on dynamics of dust-surface collisions, and on mechanisms and implications of dust spinning are discussed. Dust dynamics and transport is simulated with the DUST Transport (DUSTT) code which is tracking dust particles in 3D tokamak geometry using the forces and plasma particle and energy fluxes based on plasma and neutral-gas parameters calculated by edge-plasma transport code UEDGE. The results of dust transport simulation for current tokamaks, NSTX and DIII-D, as well as for ITER are presented. Deep penetration of dust particles toward the plasma core in tokamaks is predicted. The possible effect of dust on edge plasma performance is discussed.

1. Introduction

Dust has been observed in fusion plasmas and identified as having a potentially large impact on fusion plasmas and operation of magnetic-fusion reactors [1-7]. However, understanding of such crucial issues as: mechanisms and rates of dust production, dust dynamics in fusion plasma, impact of dust on performance of fusion devices, dust-wall interactions, is still in its infancy. Here we address some of these issues.

2. Volumetric dust growth in fusion plasmas

Under standard tokamak discharge conditions, dust particles in plasma experience net erosion or sublimation. However, in some cases (e.g., detached divertor plasmas, afterglow plasmas after discharge termination or disruption, and parasitic plasmas that occur in “shadow” regions in some tokamaks), the dust particles can grow from net deposition when low temperature plasma contains significant concentrations of intrinsic impurities. To explore the conditions necessary for volumetric dust growth, we use a simple model where the carbon-dust particle is embedded in stationary plasma (density n_e and temperatures $T_e = T_i$. The deuterium plasma contains a fixed fraction γ_c of singly-charged carbon ions $[C^+] = \gamma_c n_e$. The impact of neutrals is not considered here, so the input parameters are: n_e, T_e, and γ_c. We solve a system of coupled equations describing: i) charging of dust particle (including secondary electron and thermionic emissions); ii) energy balance of dust including plasma energy flux, radiation loss, cooling by electron emission and evaporation/sublimation (dust material temperature T_d is assumed uniform within a grain); and iii) erosion/deposition rates that include sputtering, evaporation, and sublimation as well as sticking of carbon particles to the dust. Hence, we calculate both the equilibrium T_d and the growth rate of dust particle dR_d/dt as functions of input plasma parameters (shown in Fig. 1). Since both chemical sputtering and evaporation-sublimation depend strongly on T_d, we find that dust temperatures in the range $700K < T_d < 2000K$ are favorable for deposition (chemical sputtering is suppressed while the sublimation rate remains small). But, for $T_d > 2000K$, evaporation and sublimation processes dominate.

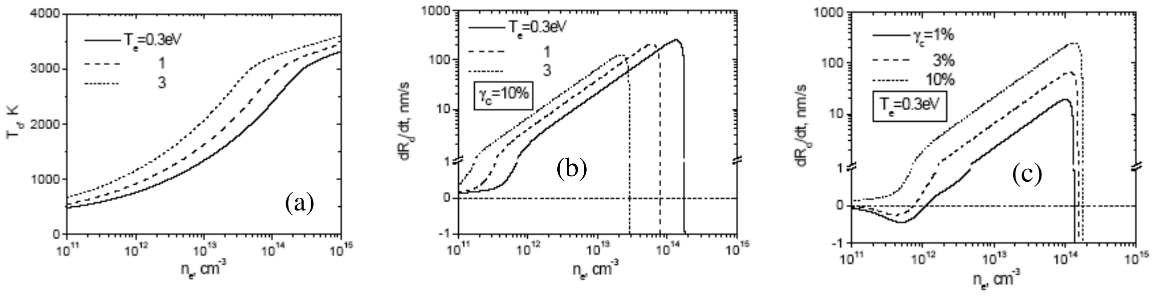

FIG. 1. Equilibrium temperature T_d and dust growth rate dR_d/dt for different plasma parameters.

The window of n_e favorable to the growth of dust is quite sensitive to plasma temperature, which controls dust heating and physical sputtering of dust. For plasma temperatures typical of detached or afterglow plasmas, $T_e \lesssim 1eV$, the window extends up to $n_e \sim 10^{14} cm^{-3}$ where the dust growth rate reaches a few hundred nm/s. Note, carbon neutrals (whose density in the detached divertor and afterglow plasmas can be comparable to or exceed the carbon ion density) should increase the dust growth rate even further.

3. Modeling of dust particle collision with material surface

Interactions of dust with material surfaces play an important role in the dynamics of dust in tokamak edge plasmas and strongly affect the penetration of dust toward the core [7]. Being accelerated by the plasma flow up to the speed about few hundred m/s, the dust particle hitting the wall can loose significant kinetic energy due to collision, chip off small bits of the wall material or be fragmented itself. Such avalanche-like generation of dust can be very dangerous for both plasma performance and safety of ITER. However, there is very limited number of experimental measurements on dust-wall interactions, especially for materials interesting for ITER, e.g. tungsten, carbon, and beryllium. Therefore here we present our preliminary and somewhat limited results of numerical simulation of Be-dust interactions with Be-wall. We model the 1-micron beryllium dust particle striking the target of 4 x 4 x 2 microns at the incident angle of 45 degrees over a range of velocities from 100 m/s to 1000 m/s using LS-DYNA, the commercial finite element program. The total simulation time is 8 ns and the particle remains in contact with the target for approximately 1 ns across the range of velocities. A total of $33x10^3$ elements were used in the calculations. The target boundaries are free. A transmitting boundary condition would be more realistic, but given the short duration of the impact, the results are probably not very sensitive to the boundary conditions. There is no friction between the particle and the target. The initial temperature is 300 K and zero ambient pressure. The simulations do not incorporate any failure models, and therefore do not allow for the possibility that the particle may fragment or that the target may generate debris. We currently do not have the necessary data, but hope to obtain it in the future. Given the large plastic deformations at 1000 m/s and the absence of a failure model these results may be questionable.

The stress tensor, $\sigma = \sigma' - PI$, is decomposed into the deviatoric stress, σ', which is described by the Steinberg-Guinan plasticity model [8,9], and the pressure, P, which calculated from the Gruneisen equation of state. The Steinberg-Guinan plasticity model was developed for high strain rates and high pressures, and the material properties were evaluated from experiments in that regime. The values of the material properties are therefore probably not optimal for the current application. The yield strength is

$$\sigma_y = \sigma_0' \left\{1 + \beta(\bar{\varepsilon}^p)^n\right\}\left\{1 + bPV^{1/3} - h(T - 300)\right\} e^{-fE_i/(E_m - E_i)} \quad (1)$$

where $\bar{\varepsilon}^p$ is the equivalent plastic strain, V is the specific volume, T is the absolute temperature in Kelvin, E_i is the internal energy, E_m is the melting energy, and the remaining variables are material constants. For beryllium we have: initial density $\rho_0 = 1.85$, initial shear modulus $G_0 = 1.51$, initial yield strength $\sigma_0' = 3.3 \times 10^{-3}$, b=26, n=0.78, b=1.54, $h = 2.56 \times 10^{-4}$, $f = 10^{-3}$, C=0.8, $S_1 = 1.124$, $S_2 = S_3 = 0$, $\gamma_0 = 1.11$, a=0, $c_p = 1.82 \times 10^{-5}$ (All parameters are in the cm-g-ms system of units). The shear modulus has a similar functional form,

$$G = G_0 \left\{1 + bPV^{1/3} - h(T - 300)\right\} e^{-fE_i/(E_m - E_i)}. \quad (2)$$

The Gruneisen equation of state with a cubic shock velocity-particle velocity defines the pressure for compressed materials as

$$P = \rho_0 C^2 \mu \left\{1 + \left(1 - \frac{\gamma_0}{2}\right)\mu - \frac{a}{2}\mu^2\right\}\left\{1 - (S_1 - 1)\mu - S_2 \frac{\mu^2}{\mu+1} - S_3 \frac{\mu^3}{(\mu+1)^2}\right\}^{-1} + (\gamma_0 + a\mu)E, \quad (3)$$

and for expanded materials, $P = \rho_0 C^2 \mu + (\gamma_0 + a\mu)E$, where C is the intercept of the shock velocity-particle velocity curve, S_1 through S_3 are the coefficients of the curve, γ_0 is the Gruneisen gamma, a is the first order volume correction to γ_0, and $\mu = (\rho/\rho_0) - 1$.

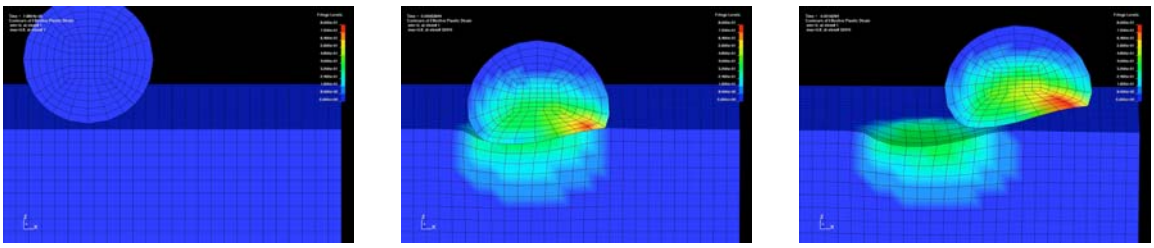

t=0.08 ns t=0.64 ns t=1.6 ns

FIG. 2. The impact sequence for the particle with an initial velocity of 1000 m/s. The colors indicate the level of plastic strain, ranging from 0.0 for the blue to 0.8 for the red.

The impact sequence for the dust particle with an initial velocity of 1000 m/s is shown in Fig. 2. The simulation results on beryllium dust particle reflectivity are summarized in Table 1. Over the range of velocities studied, the particle lost approximately 50-60% of its initial kinetic energy. The peak equivalent plastic strain in the target ranges from 0.074 to 0.398, and for the particle, the range is 0.071 to 0.848. Assuming that the system is adiabatic and neglecting the volumetric work, the temperature change as a function of the plastic strain can be approximated as $\Delta T = c_p^{-1} \int_0^{\bar{\varepsilon}^p} \sigma_y(\bar{\varepsilon}^p) d\bar{\varepsilon}^p$. Using the value of c_p from Steinberg [8], the peak temperature change ranges from 20K to 90K in the target over a velocity range of 100 m/s to 500 m/s, and for the particle, the range is 20K to 180K. For the calculation at 1000 m/s, the temperature increments for the target and particle are 240K and 560K, respectively.

V_{init} (m/s)	V_{final} (m/s)	$\frac{V_z^{final}}{V_z^{initial}}$	Normalized energy loss	Max. $\bar{\varepsilon}^p_{target}$	Max. ΔT_{target} (K)	Max. $\bar{\varepsilon}^p_{part}$	Max. ΔT^p_{part} (K)
100	72	0.345	0.486	0.044	20	0.071	20
200	138	0.340	0.524	0.107	38	0.139	56
300	196	0.274	0.573	0.146	60	0.197	94
400	255	0.274	0.593	0.168	74	0.240	127
500	316	0.253	0.601	0.189	89	0.319	182
1000	633	0.289	0.599	0.398	240	0.848	556

TABLE 1. Summary of the results on beryllium dust-surface interaction modeling.

4. Dust grain spinning due to dust-plasma interactions: mechanisms and implications

The disintegration and fragmentation of dust particles can be due to evaporation and large mechanical stresses. The later one can be due to grain heating by plasma, dust-wall interactions, and the spinning of the dust grains caused by plasma-grain interactions. Here we discuss the mechanisms of dust spinning relevant to the tokamak edge plasma and estimate the rotational frequency and its possible impact on the grain fragmentation.

The spinning of dust particles was observed in different environments ranging from laboratory to astrophysical plasmas (e.g. Ref 10). The mechanisms leading to the spinning of dust particle can be associated with: (i) shear of the plasma flow; (ii) plasma flow and asymmetry in the dust shape; (iii) synergy of the effects of electric field $\vec{E}$, plasma flow with velocity $\vec{V}_p$, and electric dipole $\vec{D}$ caused by the plasma flow.

In the presence of magnetic field, new mechanisms of dust spinning become available. In Ref. 11, it was shown that the interaction between the electric dipole, which is induced in dust grain made of insulating material by $\vec{E}\times\vec{B}$ plasma flow, and the electric field itself results in the torque, $\tau_{\vec{E}\times\vec{B}}$, acting on the grain. The torque is proportional to E^2, so that both laminar and fluctuating turbulent electric field can spin up the grain:

$$\tau_{\vec{E}\times\vec{B}} \sim \pi\langle E\rangle^2 R_d^2\rho_s \sim 4\pi^2 nTR_d\lambda_D(3\lambda_D + R_d)(k\rho_s)^2(R_d/\rho_s), \tag{4}$$

where λ_D is the Debye length, $\rho_s = C_s/\omega_{Bi}$, $\omega_{Bi} = eB/M_i c$, $C_s = \sqrt{T_e/M_i}$, and M_i is the ion mass. In Eq. (4) we assume $\lambda_D \lesssim R_d$ and estimate $\langle E\rangle^2 \sim (kT_e/e)^2$, where k is the characteristic wave number of the turbulence. In Ref. 12 the mechanisms of dust spinning are associated with: (a) gyro-motion of magnetized ions striking the grain, and (b) $\vec{j}\times\vec{B}$ force caused by cross-field current flowing through the grain due to different paths of magnetized plasma electrons and ions reaching the grain (for conducting grains). The estimation of corresponding torques for $T_i \sim T_e$ gives [12]:

$$\tau_{gyro}(R_d << \rho_s) \sim \tau_{\vec{j}\times\vec{B}} \sim nTR_d^3(R_d/\rho_s). \tag{5}$$

However, only ions with small parallel speed such that $|V_{||}|/V_{T_i} \lesssim R_d/\rho_s$ contribute to the magnitude of $\tau_{gyro}(R_d << \rho_s)$, so that the collisions of slow ions can alter the torque estimate. Taking into account the friction between plasma and spinning grain which results in the slowing down of torque (for $\lambda_D \lesssim R_d$, we have $\tau_{fric} \sim \pi nTR_d^3(\Omega_d R_d/C_s)$, where Ω_d is the dust grain angular rotation frequency), we find the stationary values of Ω_d:

$$\Omega_{ss}^{(\vec{E}\times\vec{B})} \sim 4\pi\omega_{Bi}(\lambda_D/R_d)(k\rho_s)^2 < \omega_{Bi}, \qquad \Omega_{ss}^{(gyro)} \sim \Omega_{ss}^{(\vec{j}\times\vec{B})} \sim \omega_{Bi}. \qquad (6)$$

However, to reach such steady-state values of Ω_d, the grain needs the time $t_{ss} \sim (R_d/C_s)(\rho_d/Mn) \sim 1$ s, where ρ_d is the mass density of grain material. In practice, the life-time of the grain, t_{lt}, in standard regimes of edge plasma is smaller than t_{ss} due to evaporation and collisions with the walls. Therefore, the angular rotation frequency of dust will be smaller than frequencies given in Eq. (6) by the ratio t_{lt}/t_{ss}, the magnitude of which is about 0.01 for typical values t_{lt}~0.01 s.

In order to assess the possible impact of dust spinning caused by dust-plasma interactions on dust fragmentation, we need to compare the rotational energy density, $W_d \approx 0.5 I_d \Omega_d^2 R_d^{-3}$ (where $I_d \approx \rho_d R_d^5$ is the momentum of inertia of the grain) with the critical value, W_{crit}, determined by the tensile strength of dust material. For pyrolytic graphite, $W_{crit} \sim 10^9 \mathrm{erg/cm^3}$ [13]. Then, using an estimate: $\Omega_d \sim \Omega_{ss}^{(...)} \sim \omega_{Bi}$, we find for $R_d \sim 1\,\mu m$, B~3 T, and $\rho_d \sim 2\,\mathrm{g/cm^3}$ that $\max(W_d) \sim 10^9 \mathrm{erg/cm^3}$. Since $\Omega_d < \Omega_{ss}^{(...)}$ occurs in the standard regimes of edge plasma operation, we conclude that the spinning of dust caused by dust-plasma interactions does not affect the fragmentation of carbon grains. Although, dust particles consisting of loosely bounded particulates and thus having rather low effective value of W_{crit}, can be affected by plasma induced spinning. In addition, during the main-chamber training discharges (in which the heat load on the grain is not as high as in standard tokamak discharges), the grain life-time is relatively large and the grain spinning up may strongly influence the fragmentation.

5. Modeling of dust transport and associated impurity sources in tokamak

The DUSTT code [7] is used to simulate the dust dynamics and transport in the edge plasmas and to calculate the impurity atom sources associated with dust ablation in NSTX, DIII-D, and ITER. An ensemble (~10^5) of $1\,\mu m$ carbon dust particles is launched into the plasma. The carbon influx associated with dust is taken to be the fixed fraction ξ_d of the carbon ion flux to walls calculated with UEDGE. Compared to the previous version of DUSTT, the thermionic and secondary electron emissions of dust particles are included affecting the dust particle charging, heating, and ion drag force. DUSTT calculates kinetic and potential energy fluxes from absorbed plasma particles according to OML theory accounting for the equilibrium dust charge and relative velocity of dust in plasma. A correction to the grain thermal radiation for the wavelengths $\lambda \lesssim R_d$ is introduced.

In Fig. 3, we display the 2D profiles of statistically averaged parameters of dust particles: density n_d (a), radius R_d (b), charge Q_d (c), temperature T_d (d), poloidal velocity (e), and toroidal velocity (f) obtained from the DUSTT/UEDGE modeling for typical L-mode NSTX discharge and $\xi_d = 1\%$. As one can see in Fig. 3(a and b), both dust density and averaged radius are strongly reduced in the regions with relatively dense and hot plasma (i.e. regions adjacent to the core and divertor legs). In hot plasma regions, the dust temperature is very high T_d >2500K (Fig. 3d). For such incandescent particles, strong thermionic emission results in the positive values of the dust charge Q_d (Fig. 3c). We find that the transition from negatively to positively charged dust leads to the further increase in both dust heating and sublimation rates, i.e. to the effect known as heat contraction. As follows from Fig. 3(e and f), the dust particles, being accelerated by the plasma-dust friction force due to toroidal plasma flow, reaches the speed of a few 100 m/s. We notice that toroidal components of dust velocity in Fig. 3(f) have opposite signs in the inner and outer divertors. This is due to the peculiarities of tokamak magnetic field geometry, which force the toroidal plasma flows caused by plasma recycling (and, that is, the corresponding plasma-dust drag forces) to be oppositely directed in the inner and outer divertors [14].

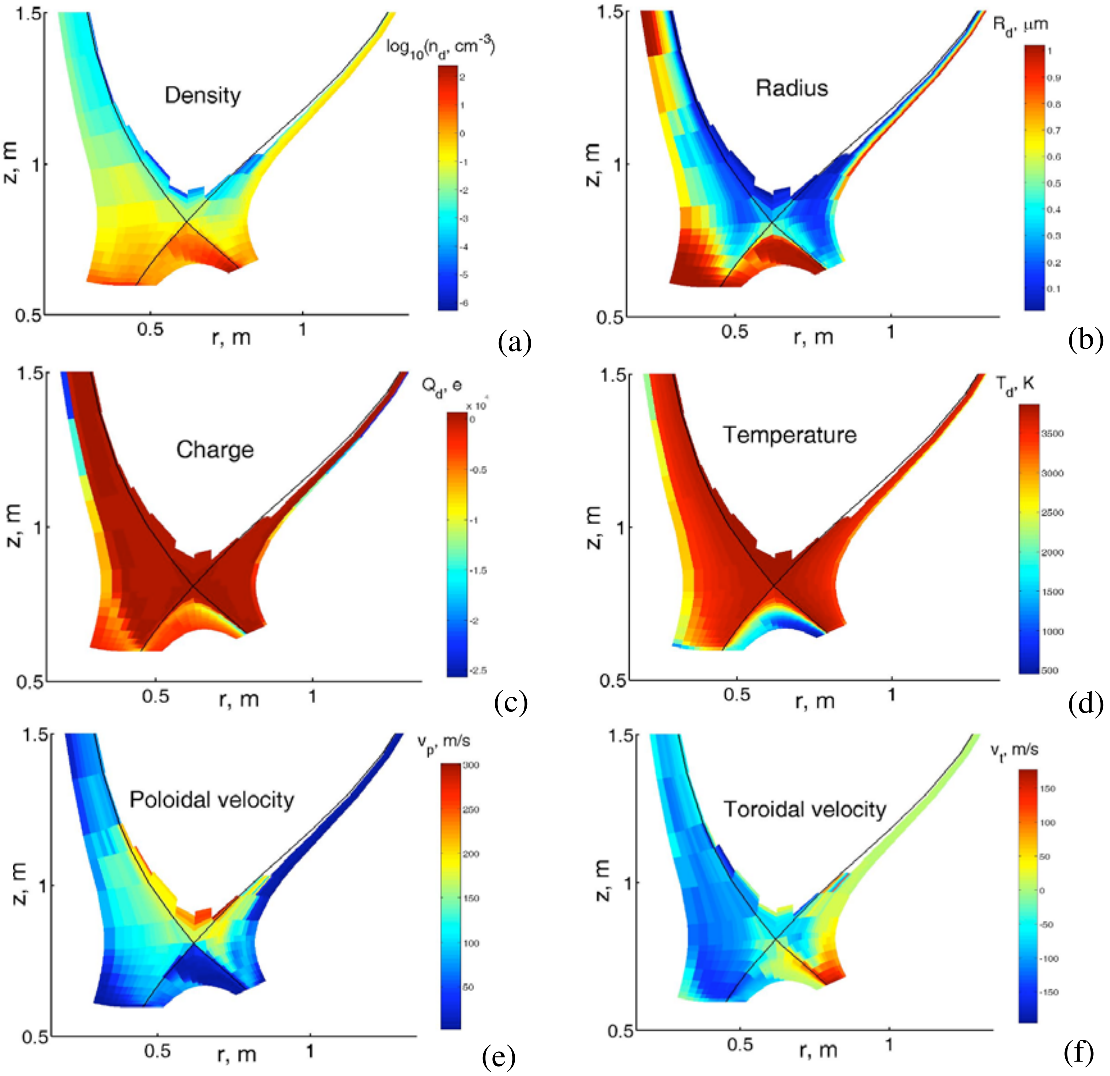

FIG.3. The 2D profiles of dust parameters calculated with DUSTT for NSTX plasma

The penetration of neutral carbon associated with dust ablation in the hot plasma is much deeper than the penetration of carbon atoms and molecules sputtered from the walls [15]. One can see this effect on Fig. 4, where we compare two contour plots of carbon atom density calculated by UEDGE for the carbon source due to sputtering by plasma ions and neutrals (top panels) and for the carbon source associated with dust ablation (bottom). Here the ablation source is calculated by DUSTT assuming that the fixed fraction $\xi_d = 1\%$ of carbon ion outflux agglomerates into the $1\,\mu m$ dust particles. Comparison is given for both NSTX (left) and ITER (right).

We use DUSTT/UEDGE package to analyze the effect of dust on the divertor plasma parameters via deeper penetration of neutral impurity toward the hot core plasma

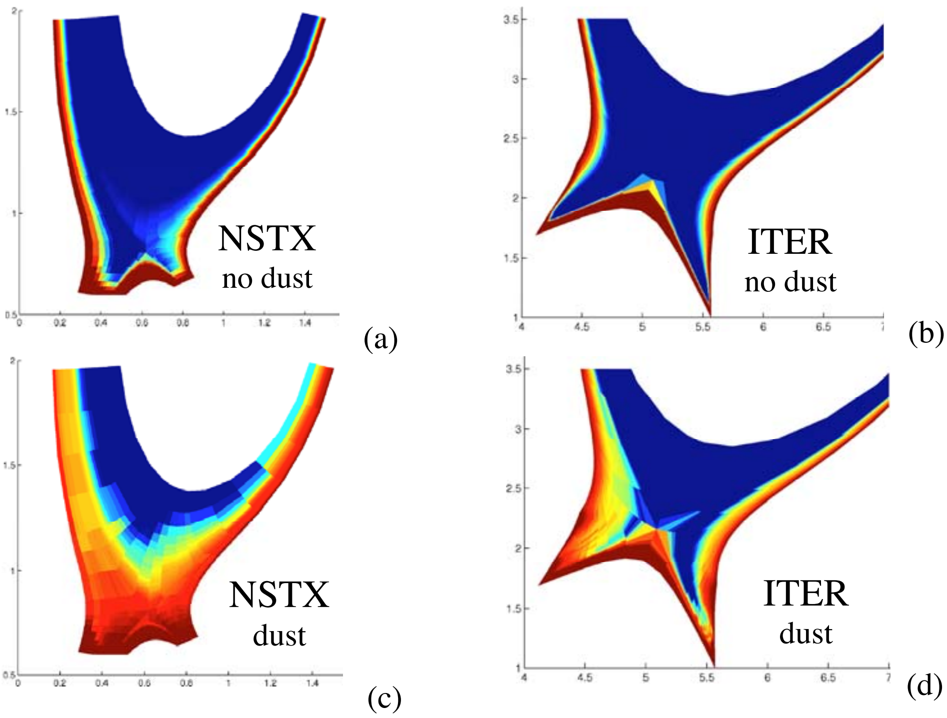

FIG. 4. Impact of dust on carbon neutral penetration for NSTX (left) and ITER (right)

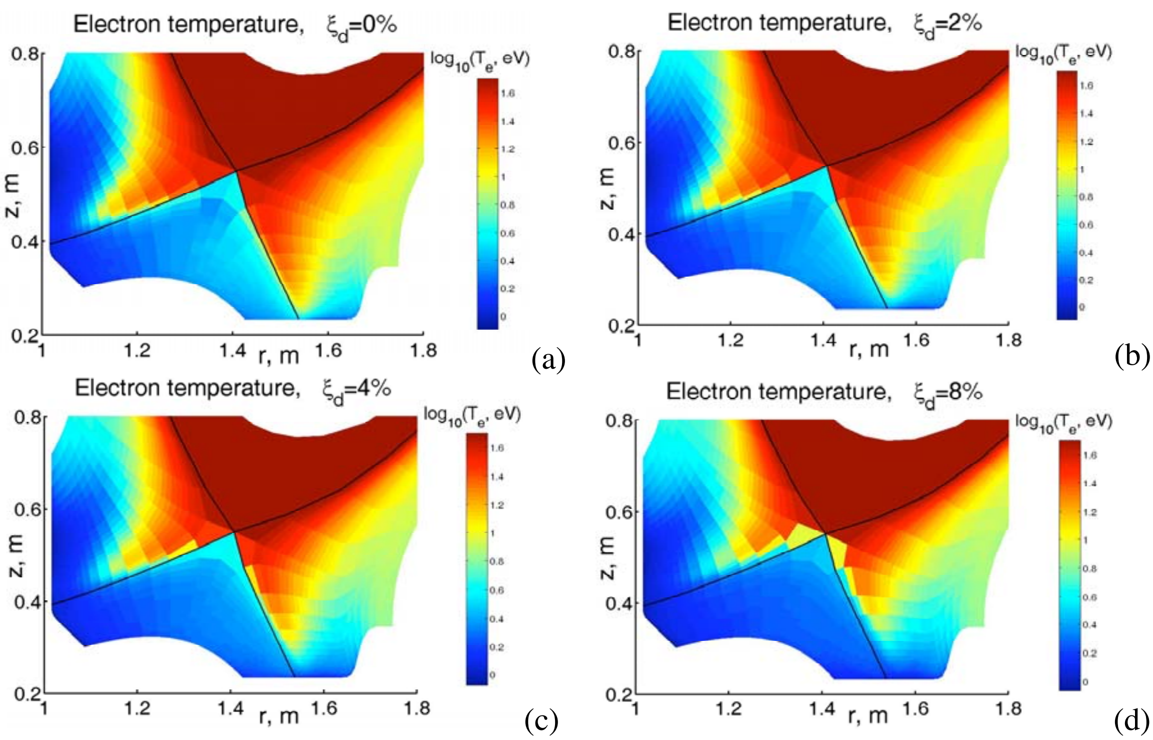

FIG. 5. Impact of dust on divertor detachment in DIII-D plasma

for L-mode shot 105517 in DIII-D. Firstly we calculate with UEDGE the plasma profiles only for carbon sputtered impurities (Fig. 5a). Then, we use DUSTT to obtain the 2D profiles of neutral carbon generation due to dust ablation for different ξ_d. Finally, we use these profiles as the fixed volumetric neutral carbon source in UEDGE and calculate new steady-state plasma profiles displayed in Fig. 5(b-d). The observed change of Te profiles highlights the progress of the outer leg detachment with increasing ξ_d.

6. Conclusions

Analysis of erosion/deposition imbalance for carbon dust particle in uniform stationary plasmas shows the possibility of volumetric dust growth when low temperature plasma contains significant concentrations of impurities. However, significant growth rate of dust, up to μm/s, is only possible in the detached divertor regimes or in the training discharges, where plasma temperature is $\lesssim 1\,\mathrm{eV}$.

We use the LS-DYNA code to simulate the reflection of $1\,\mu\mathrm{m}$ Be dust particles from the Be substrate for dust incident speeds in the range 0.1-1 km/s. Significant (~0.5) loss of kinetic energy in collision is predicted. The ratio of normal components of dust velocity after and before the collision is about 0.3. However, the simulations do not incorporate any failure models yet.

Theoretical models describing the dust spinning in tokamak plasma are developed and fast dust spinning, up to ion gyro-frequency, due to volumetric dust-plasma interactions is predicted. At the same time, we show that the spinning can result in dust fragmentation only if dust particle has cracks or consists of loosely bounded particulates.

The transport of carbon dust in tokamaks is simulated with DUSTT/UEDGE package. The statistically-averaged profiles of dust parameters are obtained for NSTX, DIII-D, and ITER. We show that dust transport causes much deeper penetration of neutral carbon than penetration of impurity atoms sputtered from walls. Deeper penetration of carbon results in higher impurity concentration, enhanced radiation loss and forces divertor detachment.

Acknowledgement. Work performed in part under auspices of USDOE by UCSD under grant DE-FG02-04ER54739 and by UC LLNL under contract W-7405-Eng-48.

References

[1] FEDERICHI, G.F., et al., Nucl. Fusion **41**, 1967 (2002)
[2] WINTER, J,, Plasma Phys. Control. Fusion **46**, B583 (2004)
[3] GORDON, C., et al., Fusion Eng. Design **55**. 347 (2001)
[4] SHARPE, J.P. ,*et al*., J. Nucl. Mater. **337-339**, 1000 (2005); **313-316**, 455 (2003)
[5] MAQUEDA, R.J., and WURDEN, G.A., Nucl. Fusion **39**, 629 (1999); COUNSELL, G.F., private communication (2004)
[6] KRASHENINNIKOV, S.I., et al., Phys. Plasmas **11**, 3141 (2004)
[7] PIGAROV, A.Yu., et al., Phys. Plasmas **12**, 122508 (2005)
[8] STEINBERG, D.J., LLNL, UCRL-MA-106439, (1996).
[9] STEINGBER, D.J., et al., J. Appl. Phys. **51**, 1498 (1980).
[10] SATO, N., in AIP Conference Proceeding 799, New York: AIP, 2005, p. 97; TSYTOVICH, V. N., SATO, N., and MORFILL, G. E., New J. Phys. **5**, 43 (2003); HUTCHINSON, I., New J. Phys. **6**, 43 (2004)
[11] KRASHENINNIKOV, S.I., SHEVCHENKO, V. I., and SHUKLA, P. K., to appear in Phys. Lett. A
[12] KRASHENINNIKOV, S.I., submitted to Phys. Plasmas
[13] MARTENS, H. E., and JAFFE, L. D., J. Appl. Phys. **31**, 1122 (1960)
[14] KRASHENINNIKOV, S.I., et al., Plasma Phys. Contr. Fusion **47**, A339 (2005)
[15] PIGAROV, A.Yu., et al., to be published in J. Nucl. Mater. (2007)